J Mater Sci (2007) 42:2557–2564
DOI 10.1007/s10853-006-1233-y

Density gradients in aluminium foams: characterisation by computed tomography and measurements of the effective thermal conductivity

E. Solórzano · M. A. Rodríguez-Pérez · J. A. Reglero · J. A. de Saja

Received: 23 August 2005 / Accepted: 26 January 2006 / Published online: 2 January 2007

Abstract The density gradients present in several aluminium foams, produced by the powder metallurgical route, have been analysed by using computed tomography and by measuring the effective thermal conductivity (λ). The method used to measure λ, Transient Plane Source (TPS) technique, allows obtaining values of the local thermal conductivity, i.e. conductivity of a localised zone within the sample. These values have been related to the density of the measured zone, which was obtained from the computed tomography experiments. A power law relationship between local effective thermal conductivity and local density has been obtained.

Introduction

In the last 10 years the fabrication routes to produce aluminium foams have been deeply studied and continuously improved [1, 2]. Nevertheless, nowadays these materials are still in-homogeneous materials, characterised by a density gradient related to both the presence of an outer skin and internal defects as, for example, a wide distribution of cell sizes, double cell walls, fractured cell walls, missing cells and cell-wall misalignments [3]. These deviations from homogeneity affect the physical properties and as a consequence an important aspect of aluminium foaming technology is to have experimental techniques able to measure these internal defects.

The cellular structure of typical aluminium foams is characterised by cells 1–3 mm in diameter and cell wall thickness from 30 to 90 μm. Computed tomography (CT) and computed micro-tomography (μCT), are non-destructive techniques that allow characterising precisely the cellular structure. Foam characteristics such as cell size, cells shape, anisotropy of pores, local density, etc. can be measured by using these techniques. Generally, μCT has been used to establish relationships between the characteristics of the cellular structure and mechanical properties or to evaluate effects of additives on the foam structure [4, 5]. Moreover, μCT has been used as a basis to create a 3D network to theoretically compute the mechanical properties [6, 7]. Eventually, μCT data can be connected with other properties, such as acoustic [8].

Thermal conductivity of metal foams has been characterised by different methods and over different cellular metals. It is important to remark that for a two phases material thermal conductivity is an effective property, in which different heat transfer mechanisms (conduction, convection and radiation) have to be considered. Several experimental investigations have dealt with this topic in the last years. Babcsán et al. [9] analysed the thermal conductivity of closed cell aluminium foams at different temperatures using a steady state method, Boemusma et al. [10] considered the influence of different fillers in the thermal conductivity of high-porosity open cell foams, the thermal conductivity of some closed cell aluminium foams with

E. Solórzano · M. A. Rodríguez-Pérez (✉) · J. A. de Saja
Dpto Física de la Materia Condensada, Facultad de Ciencias, Universidad de Valladolid, 47011 Valladolid, Spain
e-mail: marrod@fmc.uva.es

J. A. Reglero
Index. Servicios de Ingeniería, Miranda de Ebro, Spain

high-porosity was measured by Abramenko et al. [11] using a stationary method, the influence of cell size in the thermal conductivity of open cell aluminium foams with porosities in the range of 0.85–0.9 was reported by Paek et al. [12].

The cited experimental papers have mainly dealt with open cell foams of high porosity, materials with an important field of applications as heat exchangers, and with closed cell foams aluminium foams of high porosity (higher than 90%). Moreover, in all these papers the density of the foams was measured in the bulk sample, i.e. the possible effects of density gradients within the samples were not considered.

Thermal conductivity has also been analysed theoretically. Lu and Chen [13] have suggested that heat transfer is mainly due to solid conduction through cell faces and edges, neglecting radiation or convection even at high temperatures (500 °C). These authors proposed a linear relationship between density and thermal conductivity. Convection mechanisms in open cell foams, have been analysed theoretically by several authors [14, 15]. A revision of theoretical models for heat conduction in cellular materials was published by Collishaw [16].

In the present work, the effective thermal conductivity of several aluminium foams with bulk porosities in the range 70–80% has been studied using the transient plane source method (TPS). This tool permits measuring this property locally, i.e. it is possible to measure the effective thermal conductivity in specific volumes of the samples. On the other hand, CT measurements offer the possibility of calculating local density in different volumes of the same sample. The main target of the paper has been to combine these two techniques to analyse the influence that density gradients and foam homogeneity play on the effective thermal conductivity values.

Materials

Four metallic foams produced by the powder metallurgical (PM) route have been characterised. The four foams were cut from two different blocks of AlSi7 foam (Fig. 1) obtaining two couples of samples. Each sample presented four faces with outer skin and two faces in which the outer skin is not present and pore structure could be observed.

Their geometry was 60 × 65 × 65 mm and their bulk density was 0.82 and 0.88 g/cm^3 for the first couple (samples I-1 and I-2, respectively) and 0.55 and 0.63 g/cm^3 for the second couple (samples H-1 and H-2).

As it is shown in Fig. 1, gravity direction is denoted as *Z*-axis. *Y*-axis is a perpendicular direction to *Z*, from

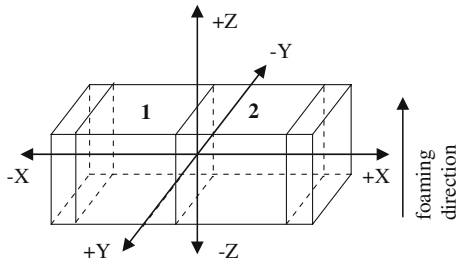

Fig. 1. Schematic configuration of the samples in the block

an outer skin to the other one. *X*-axis is perpendicular to *Y* and *Z* and connects the two faces without skin.

Samples were qualitative grouped under the criterion: *in-homogeneous sample or homogeneous sample*. This initial classification was performed by visual observation in the faces without skin and by visual observation of tomography images. Samples ''I'' presented high *in-homogeneity* in density; on the other side, the couple ''H'' presented a notable *homogeneity*. As it can be seen in Fig. 2, one of the samples ''I'' (the other one showed similar structure) present cells of a

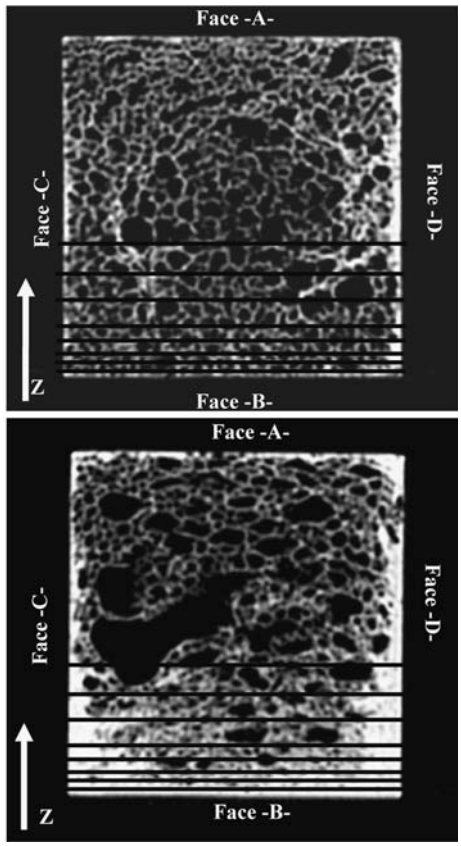

Fig. 2. Examples of the 2D slices obtained in the medical helical scanner. The face slabels and an example of intervals of analysis in the first part of *Z* axis are presented. (**a**) Sample-H- (**b**) sample-I-

high diameter and zones of high density mainly located at the bottom part the foam. On the other hand, samples ''H'' (Fig. 2) presented a regular pore size and an acceptable homogeneity in density.

Experimental techniques

Computed tomography

Principles of the helical CT technique

The principle of the helical tomography technique has been described exhaustively [17]. Its experimental implementation for medical helical scanners requires an X-ray source that is strongly collimated. For the helical CT, the X-ray tube is located in a rotating ring. A circular corona of detectors is rotated at the same time around the sample. The sample is irradiated with a X-ray beam from different angles, while it is slowly moved along the scanner axis.

A mathematic algorithm based on iterative methods is needed for the data treatment. The process output is a numeric value of the density of the pixel (in UH unities). Therefore the final output are $N \times N$ values of density, where $N \times N$ is the pixel resolution.

Experimental parameters

A helical medical scanner model Siemens Somaton operated with software VA40C was used. A final voltage of the filament of 80 KV and a current of 139 mA were used in all cases, although 100 and 120 KV were also tested. The pixel resolution was 512×512 with a slice thickness of 500 μm. Samples were placed in the scanner with the same geometric configuration they were produced (i.e. -B- face at the bottom side as it is shown in Fig. 2).

Different bending filters (mathematical filters) were tested with output images to improve image contrast and focusing obtaining different results. Finally, an *OrbiSinusSpi 2.0 H70s* filter was applied achieving optimum results for these materials.

Analysis of tomographies

One of the major difficulties in using CT is image segmentation, i.e. separation of the boundary between the metal material and the surrounding. Different methods of segmentation for different image processing techniques are proposed in the literature [18, 19]. However, for density calculation, with no micro-structural analysis, segmentation level can be obtained by imposing the condition that, after segmentation, the volume of the solid phase has to coincide with the volume of that phase calculated from the experimental bulk density.

A systematic analysis was performed along the foaming direction (Z) and along the perpendicular direction (Y). As it is shown in Table 1 and Fig. 2a and b, regions of analysis in the zones close to the skins were chosen thinner because in that part exists an abrupt density gradient.

The density of the regions of interest was obtained by:

$$\rho = \%\, V_{\mathrm{Al}} \cdot \rho_{\mathrm{Al}} + \%\, V_{\mathrm{air}} \cdot \rho_{\mathrm{air}} \quad (1)$$

where ''$\%V$'' is the volume fraction of Al/air obtained after segmentation and ρ is the density of the Al/air respectively ($\rho_{\mathrm{Al}} = 2.68$ g/cm^3, $\rho_{\mathrm{air}} = 0.012$ g/cm^3).

TPS method

Introduction to transitory methods

The TPS is a transitory method to determine the thermal conductivity (λ). All transitory methods are based on the analysis of the transient term solution of the heat conduction equation, which relates change in temperature with time. Laser flash, hot wire and transient hot strip are other techniques based on measuring the sample behaviour in the transient regime of heat flow.

These methods have several advantages in comparison with the steady-state methods. For example, it is possible to obtain values of thermal conductivity, thermal diffusivity and specific heat, simultaneously. The range of measuring of these properties is wider (0.02–400 W/mK approximately). These methods can be used to measure properties of inhomogeneous and/or anisotropic materials, offering the additional ability to measure in small samples. Furthermore, measurements are in general fast and they can be performed in localized parts of the samples.

On the other hand, it is important to remark that the TPS method is not yet standard. However, several efforts are being developed to standardise this tran-

Table 1 Intervals of density estimation

	Width of the ROI (mm)	Number of ROI's in the interval
Interval 0–6 mm	2	3
Interval 6–12 mm	3	2
Interval 12–27 mm	5	3

sient method [20]. It is also interesting to comment that in the last few years, different kinds of materials (butadiene rubber compounds, pineapple leaf fibbers reinforced composites, highly porous building materials, polymer foams and metal foams) have been characterized by using the TPS technique [21–26].

Theory of TPS method

In the TPS method a round and plane heat source is used. It behaves as a transient plane source working simultaneously as a temperature sensor. This element consists of an electrical conducting pattern of thin nickel foil (10 μm thick) in the form of double spiral, inserted between two insulating layers made of Kapton (70 μm thick), so final sensor thickness is 150 μm. The TPS element is located between two samples with both sensor faces in contact with the two samples surfaces (Fig. 3). Two samples of similar characteristics are required for this purpose.

To perform the experiments a constant electric power is supplied to the hot-disk sensor. The increase in temperature $\Delta T(t)$ is directly related to the variation in the sensor resistance $R(t)$ by the equation:

$$R(t) = R_0[1 + \alpha \Delta T(t)] \tag{2}$$

where R_0 is the disk resistance at the beginning of the recording (initial resistance) and α is the temperature coefficient of resistance of the nickel foil.

Assuming an infinite sample and the conductive pattern being in the XY plane of a coordinate system, the temperature rise at a point (XY) at time t is obtained by solving the equation for the heat conduction, which relates change in temperature with time [27, 28]. In the particular case of our sensor geometry, n concentric ring sources, the spatial average $\overline{\Delta T(\tau)}$ can be obtained through the equation:

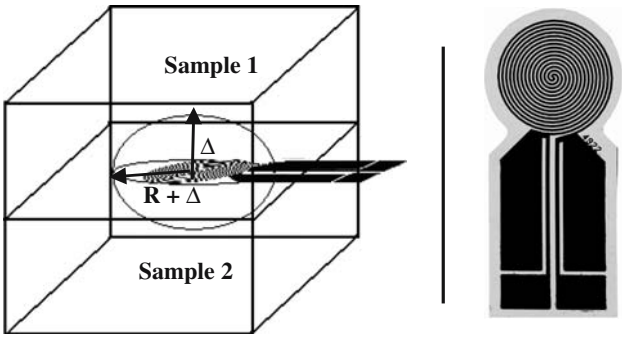

Fig. 3. Sensor (*right*) and schematic set-up of the experiments (*left*)

$$\overline{\Delta T(\tau)} = P_0(\pi^{3/2} a \cdot \lambda)^{-1} D(\tau) \tag{3}$$

where P_0 is a Bessel function, $D(\tau)$ is a geometric function characteristic of the number "n" of concentric rings, and $\overline{\Delta T(\tau)}$ is the temperature increase of the sensor expressed in terms of only one variable τ, defined as:

$$\tau = (t/\theta)^{1/2}; \quad \theta = a^2/k \tag{4}$$

where t is the measurement time from the start of the transient heating, "θ" is the characteristic time , which depends both on parameters of the sensor and the sample, "a" is the sensor radius and "k" is the thermal diffusivity of the sample.

Thermal conductivity can be obtained by fitting the experimental data to the straight line given by Eq. 2 and thermal diffusivity is calculated from Eq. 4 taking into account the τ value determined in the previous fit.

For these experiments, one of the most important parameter is named *probing depth* (Δ). This parameter gives the distance that heat flow goes over the material from any point of the disk surface. Probing depth is given by:

$$\Delta = \beta\sqrt{\kappa t} \tag{5}$$

where "β" is as a calibration constant with a value of 2.

Using the expression of the characteristic time "θ" the following equation can be obtained.

$$\Delta = \beta\sqrt{\frac{a^2 t}{\theta}} \Rightarrow \Delta \propto a t^{1/2} \tag{6}$$

consequently, modifying the *disk radius* and/or the *measurement time* it is possible to measure the thermal properties of the same sample covering different volumes (i.e. different probing depths). Therefore, it is possible to perform local measurements of the effective thermal conductivity.

Experimental

A commercial thermal constants analyser based on the TPS method model Hot Disk was used to measure the effective thermal conductivity (λ). Experiments were carried out at room temperature.

For both foams (I and H) and for each face (A, B, C, D and the 2 faces without outer skin) experiments were performed with four disks radii: 3.2, 6.4, 9.7 and 14.6 mm. Power output and measurement time were selected according to each foam face thermal characteristics.

According to the previous explanation, this means that for each foam face the effective thermal conductivity was measured under four different situations, which correspond to four different volumes covered by the heat flow (one for each sensor radii).

Five repeated experiments were performed for each experimental set-up, being the values reported in this paper the average of these five experiments. The standard deviation was lower than 3% for all the performed tests.

Analysis

The total number of points for each recording of temperature versus time curve was 200. For the effective thermal conductivity analysis, the first 40 points of each recording were discarded in calculations. This procedure reduces the effect of the contact resistance between sensor and sample.

The calculations of the thermal properties were performed according to equations reported elsewhere [27, 28] using the Hot Disk software v.5.6

Results and discussion

Density profiles

After interval analysis of tomographies and density calculations, a global profile of density along Z and Y directions was obtained for samples ''I'' and ''H''. Density values plotted are the average for each couple. As sample couples came from the same foam block, differences between samples of the same type were lower than 8% along all the density profile.

Sample ''I'' presents asymmetric profiles both in Z and Y directions. The numerical results are in agreement with the qualitative trends observed in Fig. 2, in fact for this material the density of faces B and D are clearly higher than those of faces A and C. The density asymmetry along Z direction could be associated to drainage effects [25], related to gravity along this direction. Slight asymmetry along Y direction may be related to a possible foaming asymmetric set-up of the precursor in the mould during foaming.

Sample H presents a slight asymmetric density profile along Z, probably due to gravity and a nearly symmetric profile along Y direction.

In both directions the thickness of the outer skin is clearly higher (faces B and D) for the ''I'' samples. For instance, in Z direction a constant density of 0.5 g/cm^3 is reached between 10 and 60 mm for sample ''H''. For sample ''I'' the region of constant density is smaller (between 40 and 60 mm).

The bulk density of samples, estimated by numerical integration of the profiles, was calculated and compared to the experimental bulk density. Results obtained were in close agreement with differences lower than 3% in all cases.

Effective thermal conductivity

When the TPS method is applied to measure the effective thermal conductivity of aluminium foams there are several aspects that have to be considered:

- Combining disk radii and measurement time the sample volume covered by the heat flow can be controlled.
- For homogeneous samples, different probing depths should not change the effective thermal conductivity, but in case of in-homogeneous samples, λ should be a function of the cellular structure and average density of the volume covered by the heat flow.
- As it was mentioned, one of the main targets of this paper is to inspect the changes in effective thermal conductivity when the experiments are performed with different probing depths (i.e. the heat flow reaches different volumes). Taking into account that cell size in these materials is high (1–3 mm) it is necessary to assess if the minimum probing depth which was used (6 mm approximately) is large enough to measure a real value of the effective thermal conductivity.

These three aspects have been taken into account in the analysis of the experimental results.

The values obtained in the open faces of the foams (in Fig. 5 the average value for the two faces is showed in (a) in-homogeneous foam and (b) homogeneous foam) do not depend significantly on probing depth. Bearing in mind that in this direction the foams do not have outer skins and are almost homogeneous, this result confirms that the lower probing depths used in the characterisation are high enough to give representative values of the foams thermal behaviour.

The effective conductivity measured in the faces with outer skin decreases as a function of the probing depth (Fig. 5), this can be understood in terms of the relative influence of the outer skin and foam core. As the probing depth increases the heat flow covers a higher proportion of foam core, which has a lower conductivity than the skin. As a consequence, the effective conductivity decreases. Values of effective

thermal conductivity for the lowest probing depth (sensor radius 3.2 mm –Δ = 5.7–) are much higher than values obtained with the longest sensor radius 14.6 mm. For experiments with the lowest probing depths, the conductivity can reach values similar to those of solid aluminium ($\lambda_s \approx 160$ W/mK); for instance in the experiments at the bottom face of the ''I'' sample the conductivity reached a value close to 130 W/mK.

Another interesting result is that values for sample ''I'' have a much higher dispersion (differences between faces) than those for sample H. This result is in agreement with the initial qualitative description of the samples (homogeneous and in-homogeneous). For instance, it is clear that the densest faces, -B- and -D-, showed the highest thermal conductivity. In addition, the more homogeneous foam ''H'' does not show significant differences for the faces with outer skin, which would be related to similar thickness of the skin in the different faces or, in other words, to an almost symmetric density distribution in the different directions, as it was showed in Fig. 4.

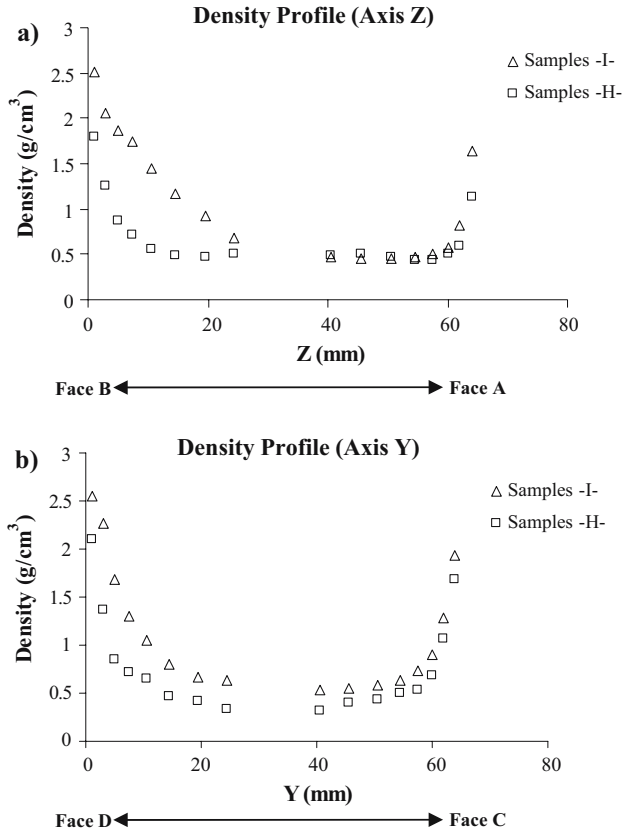

Fig. 4. Density profiles for Z and Y directions (**a** and **b**, respectively) in the two couple of samples

The thermal conductivities measured in sample ''I'' are higher than those measured in sample ''H''. This is due to the higher bulk density of the first material. A bulk thermal conductivity value, measured in the cut face, can be given for the two samples: λ_{bulk}(sample-I) = 28 W/mK, λ_{bulk}(sample-H) = 16 W/mK. These results are similar to those published by other authors and measured with other techniques [9, 11] and are in agreement with our previous results testing other aluminium foams [25, 26].

All these effects—i.e. dependence with face of measurement, sensor radius and dispersion of λ values—as it is explained in the next section, can be understood in terms of the local density of the measured region.

Relationships between local density and effective thermal conductivity

One of the problems we have had to solve in this work is to find out a method to estimate the average density of the volume reached by the heat flow. Two different mathematical implementations are proposed for this aim.

One of them only considers the Z direction, calculating the local density from a *linear integration* between $z = 0$ and $z = \Delta$:

$$\rho_{lin} = \frac{\int_{z=0}^{z=\Delta} \rho(z)\mathrm{d}z}{\int_{z=0}^{z=\Delta} \mathrm{d}z}. \tag{7}$$

The other local density estimation consists in an integration of the local density through the revolution ellipsoid that the heat flow reached during testing (Fig. 3): $z \in [0, \Delta]$ and $x, y \in [0, a + \Delta]$

$$\rho_{ellip} = \frac{\int_{x,y=0}^{x,y=a+\Delta} \int_{z=0}^{z=\Delta} \rho(z)\mathrm{d}V_{ellip}}{\int_{x,y=0}^{x,y=a+\Delta} \int_{z=0}^{z=\Delta} \mathrm{d}V_{ellip}} \tag{8}$$

The results obtained for these calculations are presented separately in Fig. 6.

It can be observed that values almost follow a linear trend as a function of the local density. The previous fact is reasonable, if we take into account that the thermal conductivity by conduction scales with density approximately as $\lambda \approx \lambda_s(\rho/\rho_s)^n$ [29], being the exponent for the materials under study close to 1 ($n \approx 1$) for densities lower than 1.5 g/cm^3 and slightly higher for the whole range of densities. According to the previous theoretical and experimental papers, radiation and convection mechanisms can be neglected [9, 13] for this kind of materials and only the conduction

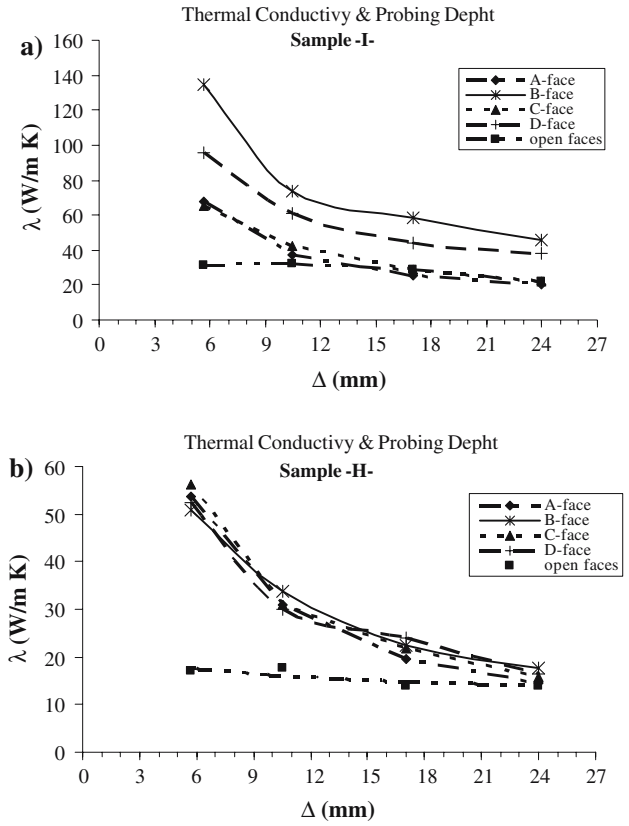

Fig. 5. Thermal conductivity as a function of the probing depth in samples (**a**) ''I'', (**b**) ''H''

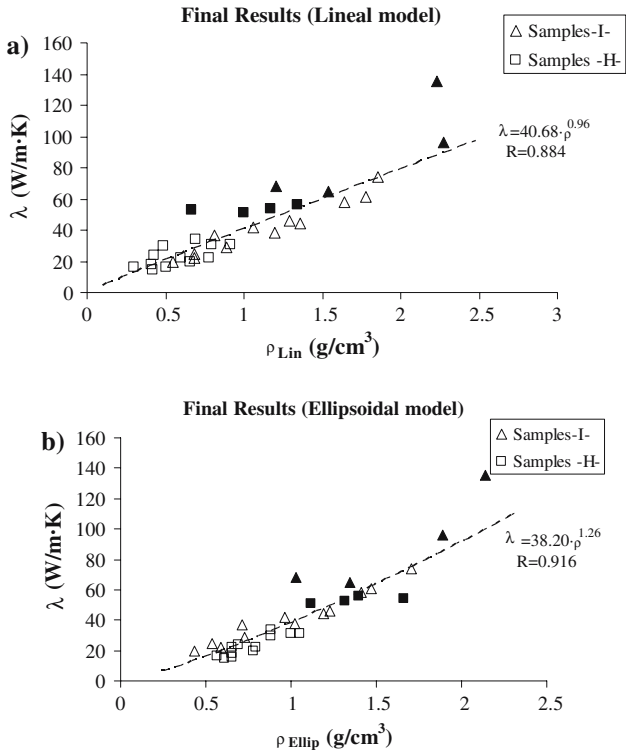

Fig. 6. Thermal conductivity as a function of the local density. (**a**) Linear model, (**b**) ellipsoidal model

mechanism has to be considered. In addition, for closed-cell aluminium foams λ_{air} is much smaller than λ_{Al} and only the solid conduction mechanism is significant, which is in agreement with our results. Consequently, only parameters of the cellular structure, such as cell shape, connectivity and topology, or the presence of the imperfections could have an influence in the thermal conductivity.

On the other hand, it is apparent that measurements of the effective thermal conductivity can be used to discriminate zones of different local densities in aluminium foams, i.e. in-homogeneities.

A closer analysis of the results of Fig. 6 shows that both models offer good results although closer results to the scaling potential law are obtained using the ellipsoidal model for density calculation. This improvement is probably related to a better-estimated average local density from the ellipsoidal model.

Finally, it is important to remark that black points in Fig. 6 represent values obtained for the disk radius of 3.2 mm. As it can be observed, these points are slightly deviated from the values obtained with longer sensors. This fact could be related with both a smaller accuracy of the λ measurements over these materials with a disk radius of comparable size to the cell size and with non-accurate density estimation for low probing depths.

Conclusions

It has been shown that metal foams produced from the powder metallurgical route present a structure characterised by considerable density gradients, and by the presence of structural in-homogeneities such as non-uniform thickness of the outer skin and presence of coarsened cells with much higher size than the average.

The TPS method can perform local or bulk measurements of the effective thermal conductivity with reproducibility and accuracy. Thermal conductivity strongly depends on density and due to this fact the TPS method can distinguish homogeneous and inhomogeneous zones of metallic foams. A power-law trend scales the effective thermal conductivity with local density.

Acknowledgments The authors are grateful to the IFAM in Bremen (D. Lehmhus) which supplied the materials of this work and to the Hospitals ''Clínico Universitario'' (Mr. César P. Zapata) and ''Pío Río Hortega'' (Mr. Ignacio Hernando), placed in Valladolid, which allowed us working with their helical scanners.

References

1. Schäffler P, Rajner W (2003) In: Banhart J, Fleck N, Mortensen A (eds) Proceedings of the 3rd international conference on cellular metals and metal foaming technology, Berlin, June 2003. Verlag Mit Publishing, Bremen, p 43
2. Körner C, Hirschmann M, Lamm M, Singer RF (2003) In: Banhart J, Fleck N, Mortensen A (eds) Proceedings of the 3rd international conference on cellular metals and metal foaming technology, Berlin, June 2003. Verlag Mit Publishing, Bremen, p 209
3. Olurin OB, Arnold M, Körner C, Singer RF (2002) Mater Sci Eng A328:334
4. Bastawros A-F, Bart-Smith H, Evans AG (2000) J Mech Phys Solids 48(Issue2):301
5. Kennedy AR, Asavavisitchai S (2004) Scripta Mater 50:115
6. Zhou J, Shrotriya P, Soboyejo WO (2004) Mech Mater 36(8):781
7. Öchsner A, Lamprecht K (2003) Mech Res Commun 30(6):573
8. Queheillalt DT, Sypeck DJ, Wadley HNG (2002) Mater Sci Eng 323(1–2):138
9. Babcsán N, Mészáros I, Hegman N (2003) Mat-wiss u. Werkstofftech 34:394
10. Boemusma K, Poulikakos D (2001) Int J Heat Mass Transf 44:827
11. Abramenko AN et al (1999) J Eng Phys Thermophys 72:369
12. Paek JW, Kang BH, Hyun JM (2000) Int J Thermophys 21(2):453
13. Lu TJ, Chen C (1999) Acta Mater 47(n.5):1469
14. Seo YK, Kang BH, Kim J-H (2001) Int J Heat Mass Transf 44:1451
15. Phanikumar MS, Mahajan RL (2002) Int J Heat Mass Transf 45:3781
16. Collishaw PG, Evans JRG (1994) J Mater Sci 29:486
17. Brink J, Heiken JP, Waug G et al (1994) Radiographies 14:887
18. Majumdar S et al (1995) Bone 14:417
19. Long DT, King MA, Sheehan J (1992) Med Phys 19:483
20. http://www.npl.co.uk/thermal/ctm/ as on 15 July 2005
21. Bouguerra A, Aït-Mokhtar A, Amiri O, Diop MB (2001) Int Commun Heat Mass Transf 28:1065
22. Saxena NS et al (1999) Eur Poly J 35:1687
23. Mangal R et al (2003) Mater Sci Eng A339:281
24. Almanza O, Rodriguez-Pérez MA, De Saja JA (2004) J Polymer Sci Part B Polymer Phys 42:1226
25. Reglero JA, Rodríguez-Perez MA et al (2003) In: Jerz J, Sêbo P, Zemánková M (eds) Proceedings of the international conference advanced metallic materials, Slovakia, November 2003. Slovak Academy of Sciences, Bratislava, p 253
26. Reglero JA, Rodríguez-Perez MA et al (2003) In: Banhart J, Fleck N, Mortensen A (eds) Proceedings of the 3th international conference on cellular metals and metal foaming technology, Berlin, June 2003. Verlag Mit Publishing, Bremen, p 499
27. Log T, Gustafsson SE (1995) Fire Mater 19(1):43
28. Gustavsson M, Karawacki E, Gustafsson SE (1994) Rev Sci Instruments 65:3856
29. Ashby MF, Evans A, Fleck N, Gibson LJ, Hutchinson JW, Wadley HNG (2000) Metal foams: a design guide. Butterworth-Heinemann, Burlington, p 47